JMEPEG (2019) 28:6219–6227
https://doi.org/10.1007/s11665-019-04380-w

1059-9495/$19.00

Ti Alloy Three-Way Pipe Fabricated by the Combination of 3D Printing and Cold Isostatic Pressing

Yanru Shao, Fang Yang, Peng Liu, Zhaohong Feng, Xin Lu, Zhimeng Guo, Huan Xu, and Alex A. Volinsky

(Submitted April 3, 2019; in revised form August 25, 2019; published online October 9, 2019)

In this study, complex-shaped Ti alloys with near-full density, using three-way pipe as an example, were achieved by the combination of 3D printing and cold isostatic pressing (CIP). A new CIP capsule consisting of porous internal support core and the external shell was prepared by 3D printing, which made it feasible to achieve internal and external co-pressing on Ti-6Al-4V powder during CIP. Therefore, complex-shaped green body was obtained with good surface quality, without obvious defects or cracks. After sintering at 1230 °C, the sintered sample had equivalent mechanical properties (hardness = 382 HV, elongation = 15.5%, tensile strength = 929 MPa and yield strength = 862 MPa) compared to the ASTMB381 standard. This study presents a novel method for fabricating complex-shaped Ti alloys with comprehensive mechanical properties.

Keywords 3D printing, cold isostatic pressing, complex-shaped, three-way pipe, Ti alloys

1. Introduction

As one of the advanced metals, titanium and titanium alloys are widely applied in the ocean, oil, gas and chemical industry (deep sea and subsea equipment) because of their high specific strength, excellent corrosion resistance and superior biocompatibility (Ref 1, 2). Generally, complex-shaped Ti alloy parts, such as valves, are one of the widely used products (Ref 3). However, the manufacturing of high-performance complex-shaped Ti alloy parts still remains challenging in actual applications due to rising raw materials costs (Ref 4) and excessive fabrication and machining costs (Ref 5, 6). The traditional methods to prepare Ti alloys are casting and forging machining. As a drawback, cast Ti alloys commonly give rise to a deficiency in terms of coarse microstructure and composition segregation, leading to relatively low mechanical performance (Ref 7-9). The range of forged machined Ti alloys applications has also been restricted due to low utilization efficiency and high processing consumption.

Over recent decades, hot isostatic pressing (HIP) technology has long been employed to obtain powder metallurgy (PM) Ti alloys with high performance as well as full densification (Ref 10-12). However, there are challenges to prepare complex-shaped steel capsules, which have to be removed after the HIP process by pickling or machining (Ref 13, 14). Furthermore, spherical Ti powders with high cost are commonly used for the HIP process (Ref 15-17). Research on how to prepare complex-shaped Ti alloys with high performance and low cost has been attracted much attention.

Cold isostatic pressing (CIP) is one of the excellent forming techniques to produce homogeneous products with high density (Ref 18, 19). As reported in Ref 20, 21, the production of Ti alloys by CIP powder consolidation followed by sintering is an emerging field with substantially reduced cost. However, the application is also limited by the shape and size of molds for preparing complex-shaped Ti alloys parts (Ref 22, 23). 3D printing is an additive manufacturing (AM) technique for fabricating a wide range of structures and complex geometries from three-dimensional (3D) model data (Ref 24, 25). It possesses the main benefits involving freedom of design, mass customization, waste minimization and the ability to manufacture complex structures (Ref 26-28). Therefore, we employed a novel technology to obtain complex-shaped Ti alloys with the combination of CIP and 3D printing. To achieve complex-shaped Ti alloy parts with near-full density, the CIP capsule needs to be reasonably designed, avoiding compacts failure. In such case, the 3D printing technology can provide the independent design possibility to unfreeze the structure and properties limitations of the complicated CIP capsule (Ref 29).

In this paper, we presented a novel method combining traditional CIP, inexpensive plastic 3D printing and unique design of compression mold to obtain complex-shaped Ti alloys parts. Taking a Ti alloy three-way pipe as an example, we demonstrated the process parameters of 3D printed CIP capsule with minimal distortion and maximum size accuracy. Then, complex-shaped samples with high performance were completely fabricated by CIP without any binder or other cumbersome process. To date, no related reports have been presented. This study unlocks the full design potential of the complex-shaped CIP capsule and the novelty of this approach can potentially be expanded into low-cost titanium industry with complex shapes.

Yanru Shao, Fang Yang, Zhaohong Feng, Xin Lu, Zhimeng Guo, and **Huan Xu**, Institute of Advanced Materials and Technology, University of Science and Technology, Beijing 100083 Beijing, China; **Peng Liu**, Department of Chemical and Materials Engineering, University of Auckland, Private Bag 92019, Auckland 1142, New Zealand; and **Alex A. Volinsky**, Department of Mechanical Engineering, University of South Florida, Tampa, FL 33620. Contact e-mails: yangfang@ustb.edu.cn and zmguo@ustb.edu.cn.

2. Experimental Procedure

2.1 Preparation

The raw material was HDH Ti-6Al-4V (TC4) powder (99.5% purity, 0.18 wt.% O). The powder morphology and particle size distribution of the Ti-6Al-4V powder are analyzed in Fig. 1. The mean particle size was about 10 μm. As shown in Fig. 2, the procedure of complex-shaped Ti alloy three-way pipe included the following main operations. To obtain a complex-shaped three-way pipe, polymeric mold capsule was printed by the MakerBot Replicator Z18 printers with thermoplastic polyurethanes (TPU) filaments. The optimal 3D printing parameters were as follows: fill ratio = 25%, shell thickness = 0.2 mm, sprayer temperature = 215 °C and printing speed = 50 mm/s. Besides, porous support inner core with threaded-in "T" shape was printed by PLA, which equipped 50% fill ratio as an upholder.

Afterward, the porous support inner core was coated by a thin layer of silicone. To obtain the silicon layer, silicone and cross-linking agent were mixed in a weight ratio of 100:3, and then it was uniformly coated on the surface of inner core. Subsequently, it was cured at ambient temperature for 24 h. The layer thickness was about 1 mm. Then, the Ti-6Al-4V powder was filled into the cavity between the coated inner core and external capsule by vibration platform under argon atmosphere. After that, the sealing and vacuuming process was performed. The sealed samples were pressed by CIP (LDJ200/1000-300YS). After pressing, the external capsule and the support inner core were dismantled. Finally, the green samples were sintered at 1230 °C for 2 h under a vacuum of 10^{-3} Pa. For comparison, common CIP samples were also prepared, in which the traditional capsule was made from commercial silica with stainless steel as the inner core.

2.2 Characterization

The sintered samples were machined and mechanically polished. Three samples for each processing condition were tested to confirm reproducibility. The sintered density was measured using the Archimedes method. The loading density was measured by the vibrometer according to the standard GB/T5162. Room temperature tensile tests were conducted using the AGI-250KN testing machine at a strain rate of 1×10^{-3} s^{-1}. The size of the test sample was in accordance with the M10 parameters without screw thread according to the ASTM E8-08 standard. The hardness of as-sintered samples was determined by vickers indenter (Krautkramer MIC10, German KK) with a load of 1 kgf for 5 s. The hardness value of the dissected three-way pipe was measured on an average of 10 points. The oxygen content of raw materials and as-sintered alloy was measured by the infrared absorption method (TCH600). The surface morphology was observed using confocal laser scanning microscope (CLSM, OLYMPUS LEXT OLS4100). The microstructure, surface morphology of the powder, and fracture were analyzed using scanning electron microscopy (SEM, Philips LEO-1450).

3. Results and Discussion

Generally, the traditional capsule was made from commercial silica with stainless steel as an inner core. After CIP, the green sample was fragmentary with cracks and defects, as

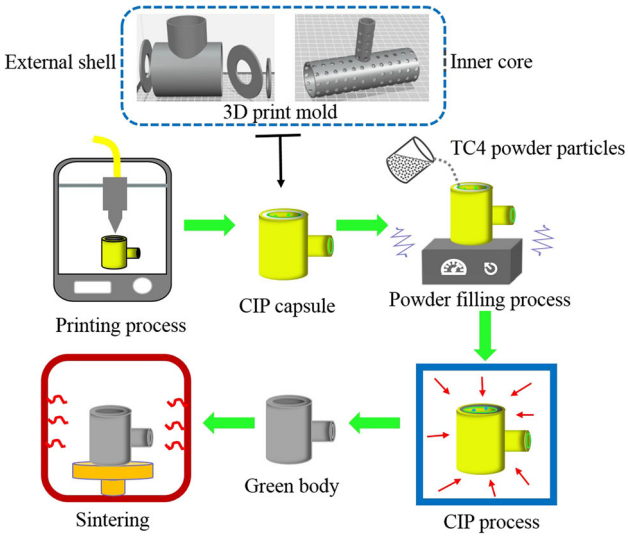

Fig. 2 The procedure of Ti alloy three-way pipe fabricated by 3D printing/CIP

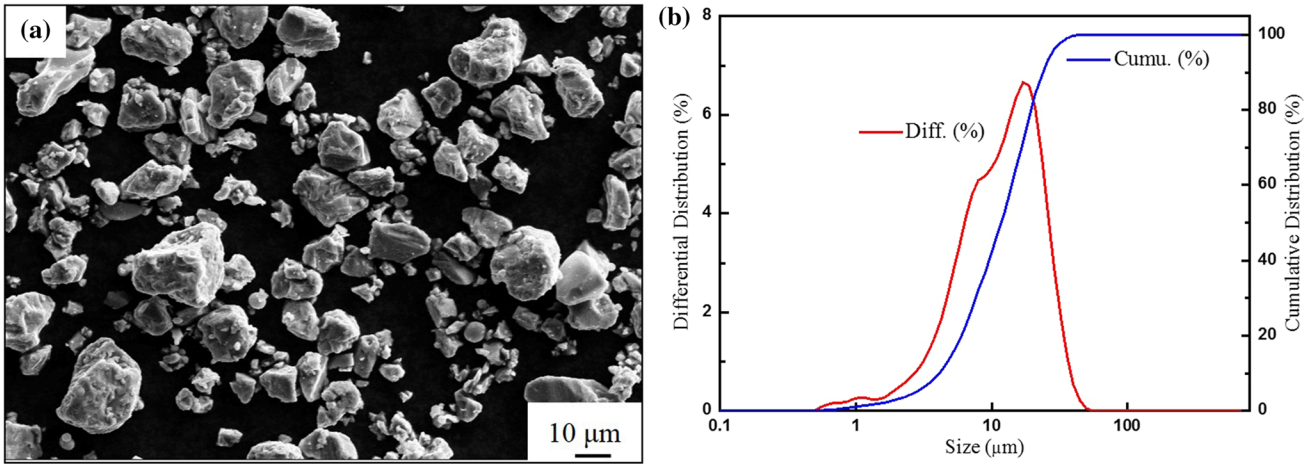

Fig. 1 (a) SEM image and (b) particle size distribution of the Ti-6Al-4V powders

shown in Fig. 3(a). The green sample fabricated by traditional CIP method had poor surface quality. In addition, the powder wasn't completely compacted, indicating poor formability of traditional CIP method. Therefore, the printed TPU mold capsule of three-way pipe was employed instead of traditional capsule. As shown in Fig. 3(b), the porous support inner core was coated with a thin silicone layer. The internal core and external shell were orderly assembled to form a CIP capsule. After CIP, three-way pipe green sample was obtained. The surface quality of the green sample was relatively good, without any defects. With the combination of internal and external co-pressing, Ti-6Al-4V powder in capsule obtained uniform pressure to maintain the designed shape. During sintering, the green sample uniformly shrank, resulting in the achievement of complex-shaped Ti alloys with good surface quality. The above results indicate that internal and external co-pressing of CIP with the combination of design freedom in capsule by 3D printing is a one promising method to obtain complex-shaped parts, as shown in Fig. 3(b).

The action mechanism of the two methods for obtaining three-way pipe is presented in Fig. 4. When the hollow-shaped tube parts were fabricated by the traditional CIP method, the inner hole was directly formed by the rigid inner core mold, as shown in Fig. 4(b). In such case, density gradients occurred during compaction, although the outer pressure was hydrostatic (Ref 30). The friction between the powders and the inner core was found to cause an uneven force acting on the powders, resulting in inhomogeneous density distribution of powder compact (Ref 31). Therefore, when the powder was compressed or displaced along the surface of the rigid core, the relative displacement was inconsistent at different positions. Furthermore, the inhomogeneous density distribution led to the production of cracks and fractures in the pressing and demolding processes, as shown in Fig. 3(a).

Conversely, when the rigid core was replaced by the perforated pipe, it allowed hydraulic oil to indirectly act on the inside Ti-6Al-4V powder, as shown in Fig. 4(b). In such case, the designed capsule enabled the hydraulic oil to work on the powder from the inside to outside simultaneously. Therefore, under the action of internal and external co-pressing, the powders were uniformly compacted with the inner and outer diameters reduced, avoiding the production of cracks and damage. Compared with the traditional CIP sample, without the restriction of the rigid core, uniform shrinkage without defects for the co-pressing CIP sample was obtained. Besides, there was no relative displacement between the powders and the inner surface of the die wall, resulting in no die wall friction. The TPU capsules fabricated by 3D printing can achieve good support for powder filling and easy removal for demolding. Beyond that, the porous capsule mold prepared by 3D printing also had high design freedom.

Due to relatively poor fluidity of fine Ti-6Al-4V powder (10 μm), a mechanical vibration was adopted for powder filling. It is common that the vibration is beneficial to promote the particles movement and rearrangement to increase the loading density. Loading density was one key parameter to obtain a whole green compact with good surface quality. Therefore, the vibrational time and frequency effect on loading density were investigated, as shown in Fig. 5. The loading density sharply increased when the vibrational time was less than 150 s, and then leveled off with a loading density of 1.54 g/cm^3 at 35 Hz. Meanwhile, the loading density firstly increased and then decreased with the increase of vibrational frequency. With the vibration carrying out, the internal friction between the particles as well as the friction between the particle and the die wall decreased after the powder particles transferred from a stationary state to a motion state (Ref 32). Consequently, more voids were filled, thereby increasing the packing density of Ti-6Al-4V powder. However, upon further increasing the vibrational frequency, the boiling and stratification phenomenon of the powder particles would appear, resulting in the loading density decreasing (Ref 33). Therefore, 150 s and 35 Hz were selected as the vibrational time and frequency to maximize the loading density. The higher powder loading density not only increased the relative density of green compact and sintered sample, but also affected the integrity of the whole part.

Furthermore, the effect of pressing pressure on the relative density was also investigated, as shown in Fig. 6. With the applied pressure increasing, the relative density gradually increased, and then basically remained unchanged after reaching 150 MPa. The optimal pressure was about 150 MPa. Respectively, the relative density of green compact was about 63.5% with a dimension size of φ52 × 66 mm^3. The shrinkage

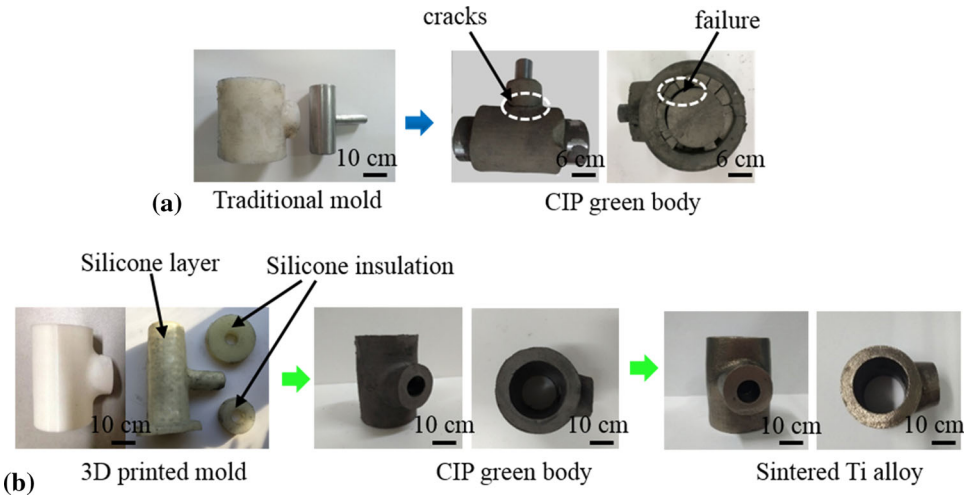

Fig. 3 Ti alloys three-way pipe fabricated by (a) traditional CIP method, and (b) 3D printing/CIP method

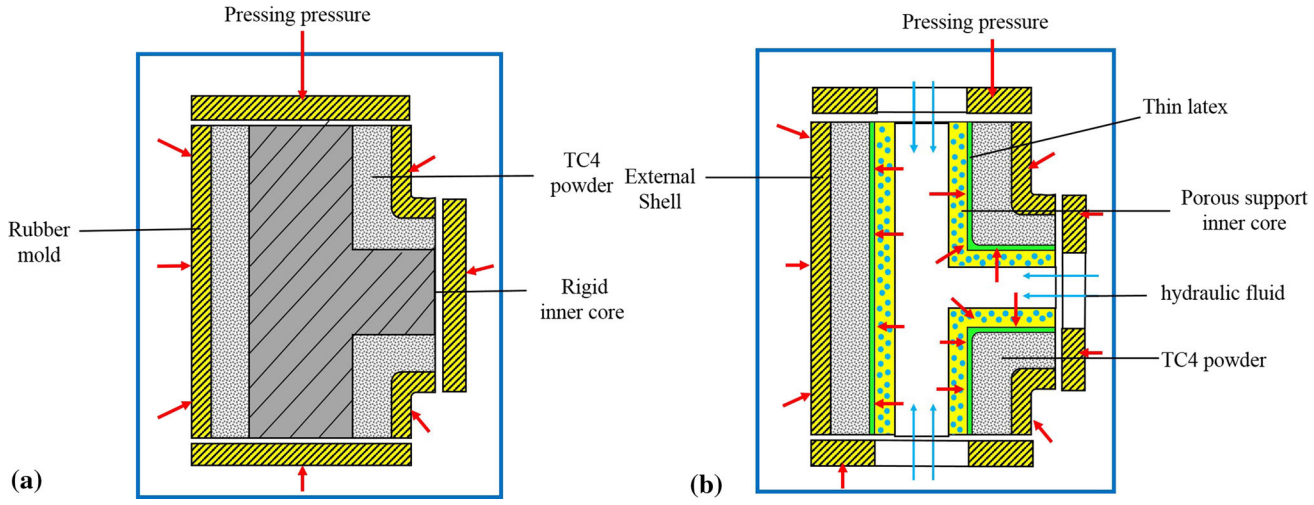

Fig. 4 The action mechanism of (a) traditional CIP method, and (b) internal and external co-pressing for CIP

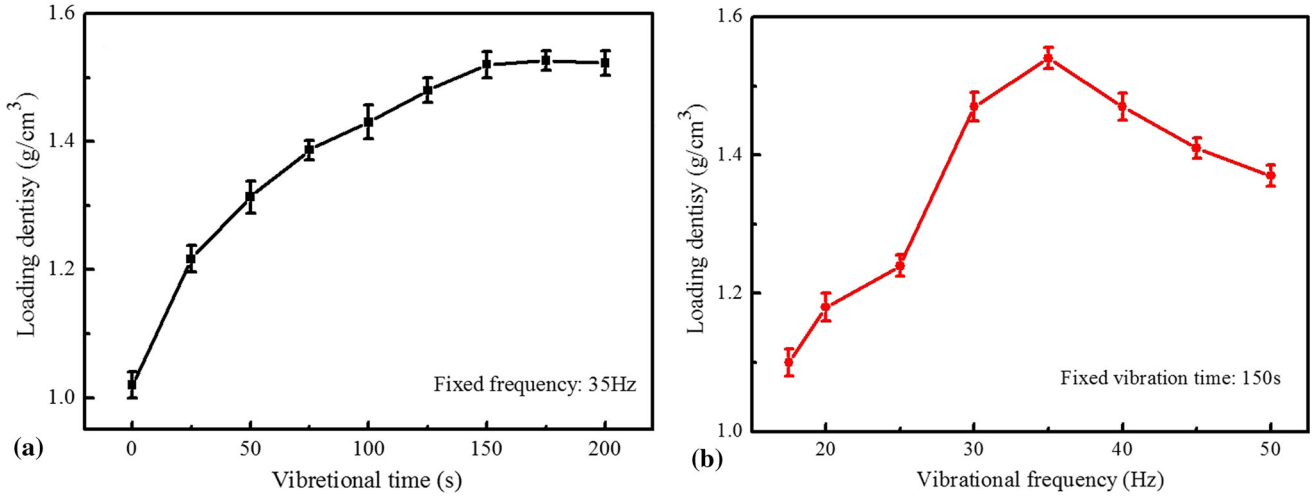

Fig. 5 The relationship curves of vibrational (a) time, and (b) frequency with loading density

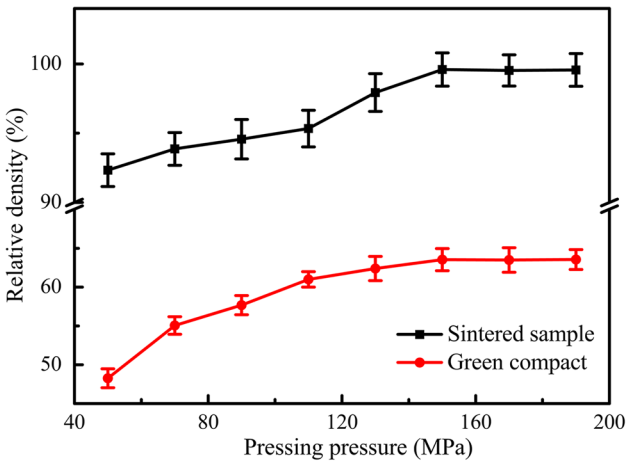

Fig. 6 The curves of relative density as a function of pressing pressure

coefficient of green compact was about 24%. After sintering at 1230 °C for 2 h, a sintered density of about 4.49 g/cm^3 was obtained, which was nearly full dense compared to the theoretical density of 4.51 g/cm^3. The size of the as-sintered sample was about φ43 × 54.5 mm^3. Accordingly, the shrinkage coefficient was about 17%.

The surface morphology of the obtained samples is presented in Fig. 7. Overall, the surface quality of the green compact and as-sintered sample was good with similar color reflections. As shown in Fig. 7(a), the surface roughness of the green compact was about 17.8 μm. The width between two adjacent lines was about 154 μm, which was much smaller than the designed layer height of 200 μm of the printed capsule. To improve the surface precision, a subsequent polishing process was carried out. After polishing by 5000# sandpaper, the surface roughness of the green body decreased to 14.1 μm. After sintering, the surface roughness of the as-sintered sample further decreased to 13.6 μm, as shown in Fig. 7(c). For comparison, the surface roughness of different parts produced by different AM processes is also listed in Table 1. On the

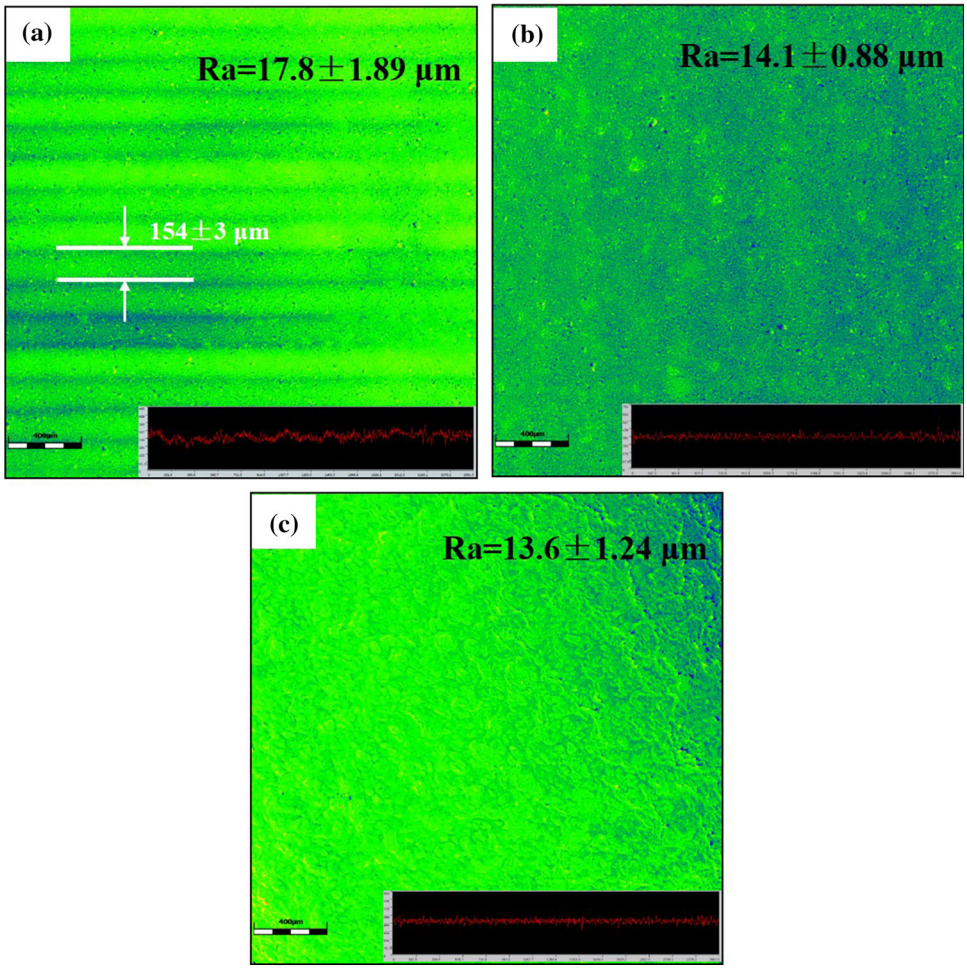

Fig. 7 CLSM images of (a) green compact, (b) green compact polished by 5000# sandpaper, and (c) as-sintered sample

Table 1 The surface roughness of different parts produced by different methods

Process	Material	Ra, μm
3D printing/CIP	Ti6Al4V	13.6
FDM (Ref 34)	ABS	24.7
SLM (Ref 35)	Ti6Al4V	20-30
MIM (Ref 36)	17-4PH	17
EBSM (Ref 37)	316L	7.9

whole, the roughness of the as-sintered sample prepared by 3D printing/CIP was relatively low.

To estimate the degree of homogeneity, the distribution of hardness was carried out, as shown in Fig. 8. The Vickers microhardness values were obtained from both sides of the Ti alloy three-way pipe. It can be seen that the degree of homogeneity of the sample was high. The hardness values of both sides were similar, ranging from 380 to 385 HV. The average value of hardness on both sides was 382 HV. It was reported that the density distribution law could be obtained indirectly from the hardness distribution (Ref 38). Therefore, this result further proved that there was no inhomogeneous density distribution in the green compact prepared by the co-pressing method.

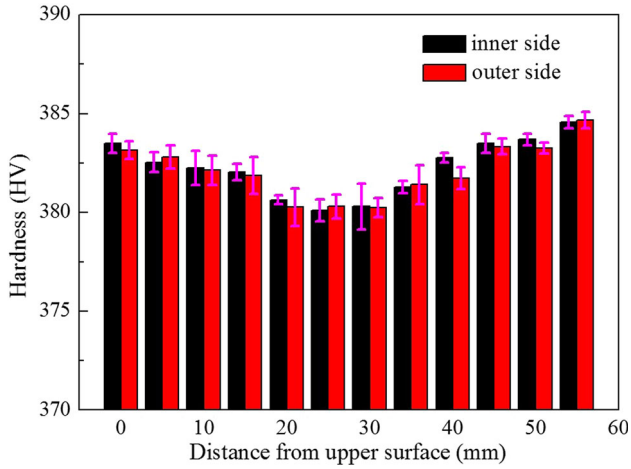

Fig. 8 Hardness distribution of the obtained Ti alloy three-way pipe

Figure 9 shows typical tensile test curves obtained from the samples sintered at 1230 °C. Furthermore, a comparison of the mechanical properties of Ti-6Al-4V alloys prepared by different methods was carried out, as summarized in Table 2. The as-sintered samples fabricated by 3D printing/CIP had comprehensive mechanical properties (elongation = 15.5%, tensile

strength = 929 MPa and yield strength = 862 MPa). The relative density of as-sintered sample was above 99.5%. Besides, the oxygen content was down to 2200 ppm due to the strict oxygen control during the preparation process. Overall, the tensile properties met the criterion required for most wrought titanium alloys in mill-annealed condition, according to the ASTMB381 standard. Besides, as shown in Table 2, the mechanical performance was comparable with the samples prepared by direct CIP followed by sintering. A similar mechanical performance was also observed in the HIP samples using spherical powder as raw material. However, although the tensile strength was encouraging in the HIP samples using HDH powder as raw material, the elongation was as low as 2%, which might be attributed to the inhomogenous microstructure and the high oxygen content (Ref 12).

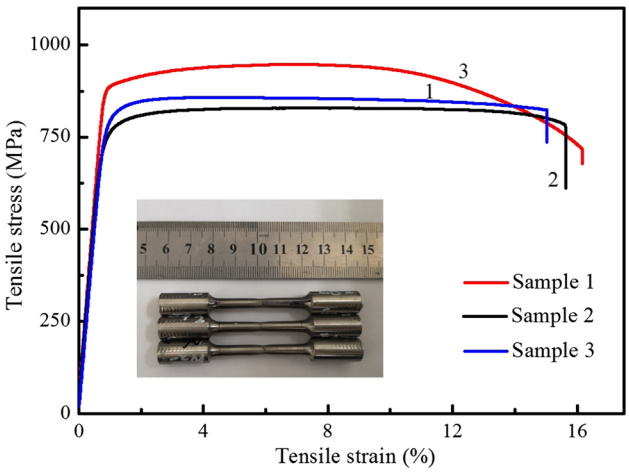

Fig. 9 The tensile engineering stress–strain curve of Ti alloys fabricated by 3D printing/CIP method

Figure 10 presents the microstructure of Ti-6Al-4V alloy sintered at 1230 °C. Homogeneous microstructure was obtained in the as-sintered sample. No cracks or pores were observed. A typical short unordered structure appeared, which contained lath-like α-phase and lamellar β-phase structures, with the length of α-phase being in the range of 10-40 μm. The lath-like α-grains in different orientations were observed. Although the sintering temperature was 1230 °C, which was much higher than the β-transus temperature, no large-scale Widmanstätten structure was observed in the matrix. The microstructure was consistent with the results reported in Ref 40. The fracture analysis of the sintered sample was also carried

Table 2 A comparison of the mechanical properties of Ti-6Al-4V alloys prepared by different methods

Preparation method	Relative density, %	Tensile strength, MPa	Yield strength, MPa	Elongation, %
3D printing/CIP/sintering	99.6 ± 0.6	929 ± 22	862 ± 37	15.5 ± 1
Wrought ASTMB381	100	895	825	10
HDH powder HIP (Ref 12)	100	1106	1044	2
Spherical powder HIP (Ref 39)	100	932	851	16.2
CIP/sintering (Ref 40)	99.5	935	865	15.8

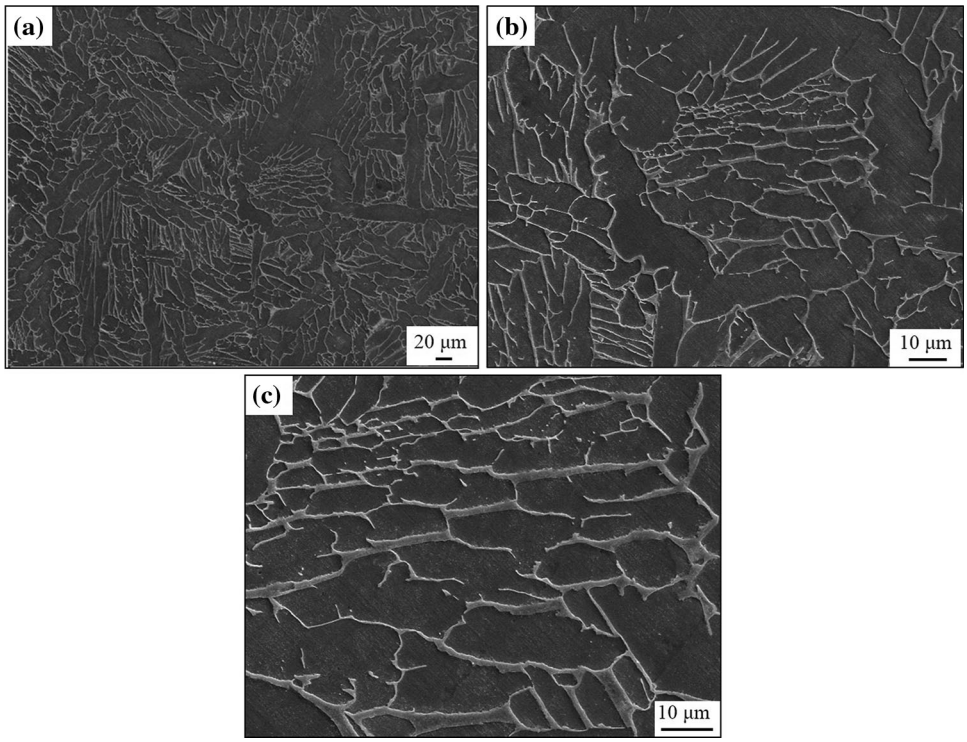

Fig. 10 SEM images of as-sintered Ti alloy under different magnifications

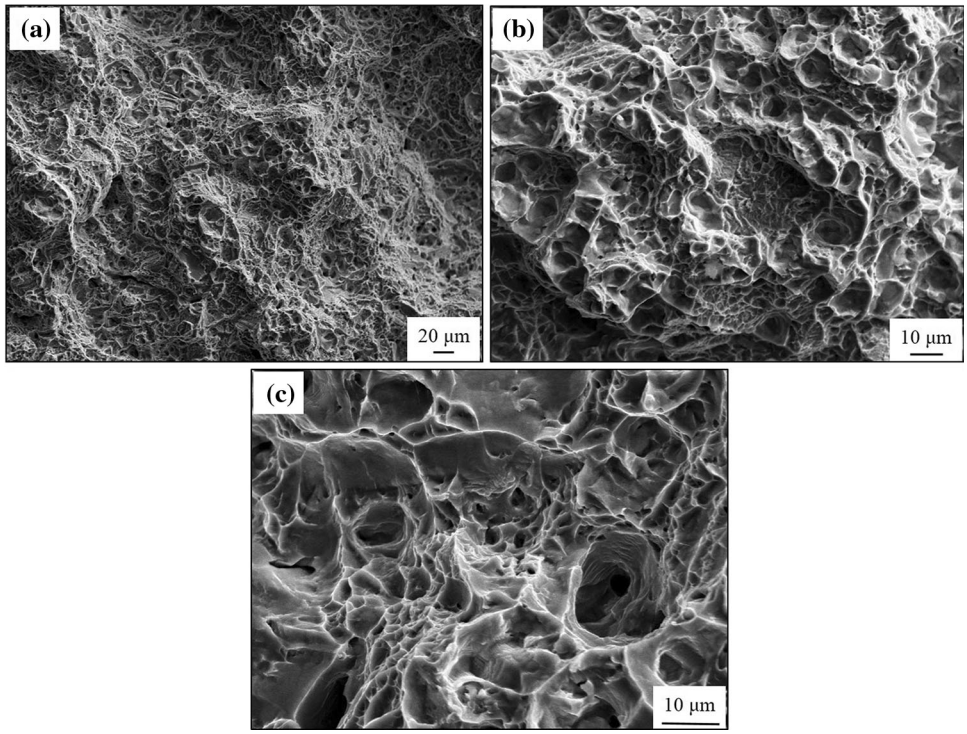

Fig. 11 Fracture morphologies of as-sintered Ti alloy under different magnifications

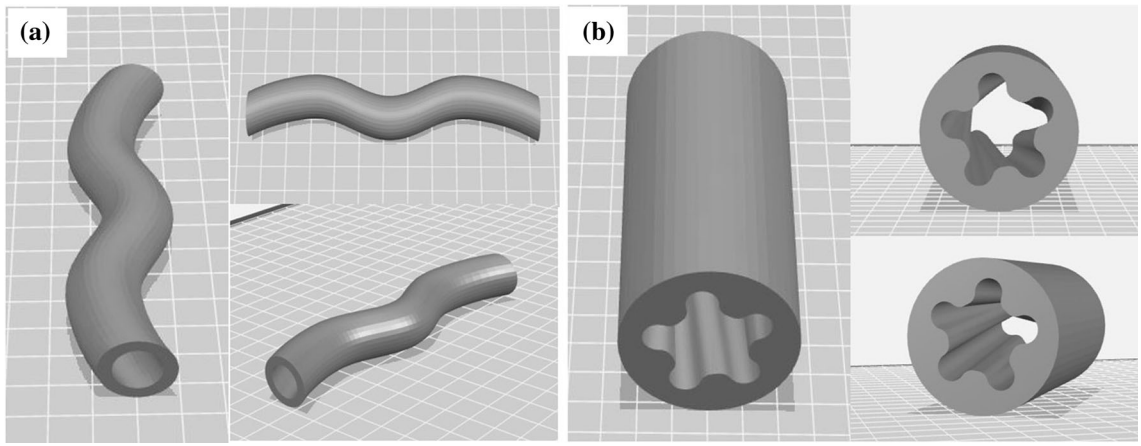

Fig. 12 Potential molds prepared by the proposed method, including (a) elbow pipe and (b) hollow tube with complex internal structure

out, as shown in Fig. 11. The fracture surface appearance presented as ductile fracture. The overall fracture mode was a typical transgranular ductile dimpled rupture with lots of dimples as well as microvoids. No evidence of inadequate bonding across prior powder particles boundaries was observed. Although the PM Ti-6Al-4V alloy was densified above the transus temperature, no large grains were formed, resulting in the obtainment of comparable ductility. Overall, the fracture appearance was consistent with the homogeneous microstructure.

Combined 3D printing with CIP, the proposed method would offer high designability to prepare complex-shaped parts with high mechanical properties. Figure 12 shows some potential molds such as elbow pipe, spiral pipe and hollow tube with complex internal structure, which can be prepared by this method to achieve good surface quality and high performance. Without inhomogeneous density distribution, green compact with homogeneous structure can be obtained. Besides, the CIP capsule can be designed to be easily removed (adjusting the soft deformation degree) without destroying the overall structure of green compact.

The above results indicated that 3D printing/CIP was one promising method to obtain complex-shaped Ti alloys with superior mechanical performance. With the employment of 3D printed CIP capsule associated with internal and external co-pressing, it was feasible to achieve highly flexible mold design and complex-shaped parts with high surface quality, which cannot be directly obtained by pressing forming. Compared

with traditional CIP method, the complex-shaped green sample was obtained with good surface quality by the proposed 3D printing/CIP method. Furthermore, the as-sintered sample had equivalent outstanding mechanical properties compared to the ASTMB381 standard, without using spherical powders as raw material. This approach can potentially be expanded into low-cost titanium industry with complex-shaped production.

4. Conclusions

Ti alloy three-way pipe was prepared by the combination of 3D printing and CIP. The CIP capsule of the three-way pipe was obtained by 3D printing, which made it feasible to achieve internal and external co-pressing for CIP. Compared to traditional CIP sample, without the restriction of the steel core, the green sample fabricated by 3D printing/CIP possessed good surface quality without cracks or damage. After being vibrated at 35 Hz for 150 s, the ideal loading density reached 1.54 g/cm^3. Correspondingly, the relative green density was 63% and the shrinkage coefficient was 24% under the pressure of 150 MPa. In addition, the relative density of the sintered sample was above 99.5%. A typical two-phase microstructure consisting of coarse α-grains and randomly distributed lath-like β-phase structure was observed in the sintered Ti-6Al-4V alloy. Meanwhile, comprehensive mechanical properties (hardness = 382 HV, elongation = 15.5%, tensile strength = 929 MPa and yield strength = 862 MPa) were obtained in the complex-shaped Ti alloy. Therefore, one promising method has been proposed to obtain complex-shaped Ti alloys with high mechanical properties.

Acknowledgments

This work was supported by the China Postdoctoral Science Foundation (No. 2018M641188), the Fundamental Research Funds for the Central Universities. (No. FRF-TP-17-032A1) and the National Key R&D Program of China (No. 2016YFB1101201).

References

1. H. Paydas, A. Mertens, R. Carrus, J. Lecomte-Beckers, and J.T. Tchuindjang, Laser Cladding as Repair Technology for Ti-6Al-4V Alloy: Influence of Building Strategy on Microstructure and Hardness, *Mater. Des.*, 2015, **85**, p 497–510
2. H.S. Tran, J.T. Tchuindjang, H. Paydas, A. Mertens, R.T. Jardin, L. Duchêne, R. Carrus, J. Lecomte-Beckers, and A.M. Habraken, 3D Thermal Finite Element Analysis of Laser Cladding Processed Ti-6Al-4V Part with Microstructural Correlations, *Mater. Des.*, 2017, **128**, p 130–142
3. M. Fröend, F. Fedor, S. Riekehr, P. Alvarez, F. Zubiri, S. Bauer, B. Klusemann, and N. Kashaev, Fiber Laser Welding of Dissimilar Titanium (Ti-6Al-4V/cp-Ti) T-Joints and their Laser Forming Process for Aircraft Application, *Opt. Laser Technol.*, 2017, **96**, p 123–131
4. P. Sun, Z.Z. Fang, M. Koopman, J. Paramore, K.S.R. Chandran, Y. Ren, and J. Lu, An Experimental Study of the (Ti-6Al-4V)-xH Phase Diagram Using In Situ Synchrotron XRD and TGA/DSC Techniques, *Acta Mater.*, 2015, **84**, p 29–41
5. G.A. Wen, P. Cao, B. Gabbitas, D.L. Zhang, and N. Edmonds, Development and Design of Binder Systems for Titanium Metal Injection Molding, An Overview, *Metall. Mater. Trans. A*, 2012, **44**, p 1530–1547
6. P. Sun, Z.Z. Fang, Y. Xia, Y. Zhang, and C.S. Zhou, A Novel Method for Production of Spherical Ti-6Al-4V Powder for Additive Manufacturing, *Powder Technol.*, 2016, **301**, p 331–335
7. P. Sun, Z.Z. Fang, and M. Koopman, A Comparison of Hydrogen Sintering and Phase Transformation (HSPT) Processing with Vacuum Sintering of CP-Ti, *Adv. Eng. Mater.*, 2013, **15**, p 1007–1013
8. A. Dehghan-Manshadi, D. StJohn, M. Dargusch, Y. Chen, J.F. Sun, and M. Qian, Metal Injection Moulding of Non-spherical Titanium Powders, Processing, Microstructure and Mechanical Properties, *J. Manuf. Process.*, 2018, **31**, p 416–423
9. M. Ahmed, D.G. Savvakin, O.M. Ivasishin, and E.V. Pereloma, The Effect of Thermo-Mechanical Processing and Ageing Time on Microstructure and Mechanical Properties of Powder Metallurgy near β Titanium Alloys, *J. Alloys Compd.*, 2017, **714**, p 610–618
10. C. Cai, X.Y. Gao, Q. Teng, M. Li, K.K. Pan, B. Song, C.Z. Yan, Q.S. Wei, and Y.S. Shi, A Novel Hybrid Selective Laser Melting/Hot Isostatic Pressing of Near-Net Shaped Ti-6Al-4V Alloy Using an In Situ Tooling: Interfacial Microstructure Evolution and Enhanced Mechanical Properties, *Mater. Sci. Eng. A*, 2018, **717**, p 95–104
11. X.X. Li, C. Yang, T. Chen, Z.Q. Fu, Y.Y. Li, O.M. Ivasishin, and E.J. Lavernia, Hot Deformation Behavior of the Ti6Al4V Alloy Prepared by Powder Hot Isostatic Pressing, *Scr. Mater.*, 2018, **151**, p 47–52
12. Y. Kim, E.P. Kim, Y.B. Song, S.H. Lee, and Y.S. Kwon, Microstructure and Mechanical Properties of Hot Isostatically Pressed Ti-6Al-4V Alloy, *J. Alloys Compd.*, 2014, **603**, p 207–212
13. C. Cao, B. Song, Q.S. Wei, Y. Wu, P.J. Xue, and Y.S. Shi, Effect of Tooling Material on the Internal Surface Quality of Ti6Al4V Parts Fabricated by Hot Isostatic Pressing, *Metall. Mater. Trans. A*, 2017, **48**, p 34–38
14. C. Cai, B. Song, C.L. Qiu, L.F. Li, P.J. Xue, Q.S. Wei, J.X. Zhou, H. Nan, H.X. Chen, and Y.S. Shi, Hot Isostatic Pressing of In Situ TiB/Ti-6Al-4V Composites with Novel Reinforcement Architecture, *J. Alloys Compd.*, 2017, **710**, p 364–374
15. J. Wu, R.P. Guo, L. Xu, Z.G. Lu, Y.Y. Cui, and R. Yang, Effect of Hot Isostatic Pressing Loading Route on Microstructure and Mechanical Properties of Powder Metallurgy Ti_2AlNb Alloys, *J. Mater. Sci. Technol.*, 2017, **33**, p 172–178
16. M.N. Rahaman, R.E. Dutton, and S.L. Semiatin, Fabrication of Dense Thin Sheets of γ-TiAl by Hot Isostatic Pressing of Tape-Cast Monotapes, *Mater. Sci. Eng. A*, 2003, **360**, p 169–175
17. V. Samarov, D. Seliverstov, and F.H. Froes, Fabrication of near-net-shape cost-effective titanium components by use of prealloyed powders and hot isostatic pressing, Titanium Powder Metal., 2015, p 313-336
18. Z.J. Wang, Y.S. Shi, W.T. He, K. Liu, and Y.S. Zhang, Compound Process of Selective Laser Processed Alumina Parts Densified by Cold Isostatic Pressing and Solid State Sintering: Experiments, Full Process Simulation and Parameter Optimization, *Ceram. Int.*, 2015, **41**, p 3245–3253
19. F. Heidari, M. Razavi, M. Ghaedi, M. Forooghi, M. Tahriri, and L. Tayebi, Investigation of Mechanical Properties of Natural Hydroxyapatite Samples Prepared by Cold Isostatic Pressing Method, *J. Alloys Compd.*, 2017, **693**, p 1150–1156
20. S.M. El-Soudani, K.O. Yu, and E.M. Crist, Optimization of Blended-Elemental Powderbased Titanium Alloy Extrusions for Aerospace Applications, *Metall. Mater. Trans. A*, 2013, **44**(2), p 899–910
21. S.M. El-Soudani, M. Campbell, J. Phillips, T. Esposito, V. Moxson, and V. Duz, *Canless Extrusion Process Development for Blended-Elemental Powder-based Titanium Ti-6AL-4V Alloy, AeroMat*, Austin, Texas, 2008
22. C.S. Lin and S.T. Lin, Effects of Granule Size and Distribution on the Cold Isostatic Pressed Alumina, *J. Mater. Process. Technol.*, 2008, **201**, p 657–661
23. D. Tadic and M. Epple, Mechanically Stable Implants of Synthetic Bone Mineral by Cold Isostatic Pressing, *Biomaterials*, 2003, **24**, p 4565–4571
24. T.D. Ngo, A. Kashani, G. Imbalzano, K.T.Q. Nguyen, and D. Hui, Additive Manufacturing (3D Printing): A Review of Materials, Methods, Applications and Challenges, *Compos. Part B Eng.*, 2018, **143**, p 172–196
25. V. Chastand, P. Quaegebeur, W. Maia, and E. Charkaluk, Comparative Study of Fatigue Properties of Ti-6Al-4V Specimens Built by Electron Beam Melting (EBM) and Selective Laser Melting (SLM), *Mater. Charact.*, 2018, **143**, p 76–81

26. L. Santana, J.L. Alves, and A.C.S. Netto, A Study of Parametric Calibration for Low Cost 3D Printing: Seeking Improvement in Dimensional Quality, *Mater. Des.*, 2017, **135**, p 159–172
27. H.Z. Zhong, X.Y. Zhang, S.X. Wang, and J.F. Gu, Examination of the Twinning Activity in Additively Manufactured Ti-6Al-4V, *Mater. Des.*, 2018, **144**, p 14–24
28. M. Bodaghi, A.R. Damanpack, G.F. Hu, and W.H. Liao, Large Deformations of Soft Metamaterials Fabricated by 3D Printing, *Mater. Des.*, 2017, **131**, p 81–91
29. R. Lu, S. Chandrasekaran, W.L.D. Frane, R.L. Landingham, M.A. Worsley, and J.D. Kuntz, Large Deformations of Soft Metamaterials Fabricated by 3D Printing, *Mater. Des.*, 2018, **148**, p 8–16
30. M. Reiterer, T. Kraft, U. Janosovits, and H. Riedel, Finite Element Simulation of Cold Isostatic Pressing and Sintering of SiC Components, *Ceram. Int.*, 2004, **30**(2), p 177–183
31. K.T. Kim and H.T. Lee, Effect of Friction Between Powder and a Mandrel on Densification of Iron Powder during Cold Isostatic Pressing, *Int. J. Mech. Sci.*, 1998, **40**(6), p 507–519
32. R.B. Canto, V. Tita, J.D. Carvalho, and B.D.M. Purquerio, Finite Element Simulation of Ceramic Powder Isostatic Pressing Process Using Material Parameters for Uniaxial Compaction, *Mater. Sci. Forum*, 2003, **416–418**, p 561–566
33. W.T. He, Q.S. Wei, K. Liu, Y.S. Shi, and J. Liu, Numerical Simulation of Cold Isostatic Pressed Alumina Parts Produced by Selective Laser Sintering and Part Shape Optimization, *Ceram. Int.*, 2013, **39**, p 9683–9690
34. C.J.L. Perez, Analysis of the Surface Roughness and Dimensional Accuracy Capability of Fused Deposition Modeling Process, *Int. J. Prod. Res.*, 2001, **40**, p 2865–2881
35. P. Edwards and M. Ramulu, Fatigue Performance Evaluation of Selective Laser Melted Ti-6Al-4V, *Mater. Sci. Eng. A*, 2014, **598**, p 327–337
36. L. Liu, X.D. Wang, X. Li, X.T. Qi, and X.H. Qu, Effects of Size Reduction on Deformation, Microstructure, and Surface, Roughness of Micro Components for Micro Metal Injection Molding, *Int. J. Miner. Metall. Mater.*, 2017, **24**(9), p 1022–1026
37. C. Guo, F. Lin, and W. Ge, Study on the Fabrication Process of 316L Stainless Steel via Electron Beam Selective Melting, *Chin. J. Mech. Eng.*, 2014, **50**, p 152–153
38. H.G. Kim, J.W. Lee, and K.T. Kim, The Effect of a Rubber Mold on Densification and Deformation of a Metal Powder Compact during Cold Isostatic Pressing, *Mater. Sci. Eng. A*, 2001, **318**(1–2), p 174–182
39. R. Guo, L. Xu, J. Wu, R. Yang, and B.Y. Zong, Microstructural Evolution and Mechanical Properties of Powder Metallurgy Ti-6Al-4V Alloy based on Heat Response, *Mater. Sci. Eng. A*, 2015, **639**, p 327–334
40. C. Zhang, B.X. Lu, H.Y. Wang, Z.M. Guo, V. Paley, and A.A. Volinsky, Vacuum Pressureless Sintering of Ti-6Al-4V Alloy with Full Densification and Forged-Like Mechanical Properties, *J. Mater. Eng. Perform.*, 2018, **27**, p 282–292